JOURNAL OF TISSUE ENGINEERING AND REGENERATIVE MEDICINE
J Tissue Eng Regen Med (2013)
Published online in Wiley Online Library (wileyonlinelibrary.com) **DOI:** 10.1002/term.1810

RESEARCH ARTICLE

Design and validation of a dynamic cell-culture system for bone biology research and exogenous tissue-engineering applications

Alexander C. Allori[1,5], Edward H. Davidson[1], Derek D. Reformat[1], Alexander M. Sailon[1], James Freeman[4], Adam Vaughan[4], David Wootton[4], Elizabeth Clark[3], John L. Ricci[2] and Stephen M. Warren[1]*
[1]*Institute of Reconstructive Plastic Surgery, New York University Medical Center, New York, NY, USA*
[2]*Department of Biomaterials and Biomimetics, New York University College of Dentistry, New York, NY, USA*
[3]*Department of Chemical Engineering, Oklahoma State University, Oklahoma, OK, USA*
[4]*Albert Nerken School of Engineering, Cooper Union for the Advancement of Science and Art, New York, NY, USA*
[5]*Division of Plastic, Maxillofacial & Oral Surgery, Duke University Hospital, Durham, NC, USA*

Abstract

Bone lacunocanalicular fluid flow ensures chemotransportation and provides a mechanical stimulus to cells. Traditional static cell-culture methods are ill-suited to study the intricacies of bone biology because they ignore the three-dimensionality of meaningful cellular networks and the lacunocanalicular system; furthermore, reliance on diffusion alone for nutrient supply and waste product removal effectively limits scaffolds to 2–3 mm thickness. In this project, a flow-perfusion system was custom-designed to overcome these limitations: eight adaptable chambers housed cylindrical cell-seeded scaffolds measuring 12 or 24 mm in diameter and 1–10 mm in thickness. The porous scaffolds were manufactured using a three-dimensional (3D) periodic microprinting process and were composed of hydroxyapatite/tricalcium phosphate with variable thicknesses, strut sizes, pore sizes and structural configurations. A multi-channel peristaltic pump drew medium from parallel reservoirs and perfused it through each scaffold at a programmable rate. Hermetically sealed valves permitted sampling or replacement of medium. A gas-permeable membrane allowed for gas exchange. Tubing was selected to withstand continuous perfusion for $>$ 2 months without leakage. Computational modelling was performed to assess the adequacy of oxygen supply and the range of fluid shear stress in the bioreactor–scaffold system, using 12 $\times$ 6 mm scaffolds, and these models suggested scaffold design modifications that improved oxygen delivery while enhancing physiological shear stress. This system may prove useful in studying complex 3D bone biology and in developing strategies for engineering thick 3D bone constructs.

Received 7 February 2012; Revised 20 January 2013; Accepted 22 July 2013

Keywords **tissue engineering; bone; lacunocanalicular system; bioreactor; cell culture; scaffold; fluid shear stress**

1. Introduction

To date, bone biology research has largely considered cellular biology, the biochemical environment and biomechanical stimuli as distinct and separate entities. In nature, of course, these processes are closely related and interdependent. It is likely that successful tissue-engineering strategies will require the biomimetic synthesis of these three aspects in their design and implementation. We hypothesize that, by recreating the three-dimensional (3D) bony architecture *in vitro* and by providing appropriate biochemical and biomechanical cues present in native bone, we will also be able to replicate bone's natural biology.

Growing bone *in vitro* is not without its challenges, however. Bone is inherently a 3D structure. Its cells are imprisoned in a solid matrix, making *in situ* study or cellular extraction difficult. These isolated cells

*Correspondence to: S. M. Warren, Institute of Reconstructive Plastic Surgery, New York University Medical Center, 560 First Avenue, TH-169, New York, NY 1001, USA. E-mail: stephen.warren.md@gmail.com

survive by chemotransportation through a dedicated lacunocanalicular network, and they also sense and respond to external mechanical forces via the fluid shear stresses generated by oscillatory flow within this same network (Allori *et al.*, 2008a; Cowin *et al.*, 1991; Fritton *et al.*, 2000; Weinbaum *et al.*, 1994; Weinbaum *et al.*, 2001). Traditional two-dimensional (2D), static cell-culture methods are ill-suited to study the intricacies of bone biology because they ignore the three-dimensionality of meaningful cellular networks and the importance of the lacunocanalicular system.

3D *in vitro* bone biology research and engineering requires the development of novel scaffolds on which cells may be cultured. Intuitively, the ideal biomaterial should be a biomimetic reproduction of the matrix of native bone. The inorganic element of the natural bone matrix consists of mainly crystalline mineral salts in the form of hydroxyapatite {HA; $(Ca_{10}[PO_4]_6)(OH)_2$} (Allori *et al.*, 2008b). In addition to providing the 'raw materials' for mineralized matrix formation, HA has a nanoscale topography that promotes cellular adhesion, differentiation, growth and proliferation. For these reasons, many groups have advocated the use of HA scaffolds in regenerating bone *in vivo* (Gosain *et al.*, 2002; Nguyen *et al.*, 2009; Simon *et al.*, 2007, 2008) and *in vitro* (Scherberich *et al.*, 2007).

While in 2D culture cells are in continuous contact with surrounding culture medium and diffusion is sufficient to maintain the cells, diffusion alone is inadequate to support the central pulp of a thick 3D tissue-engineered construct. Prior studies have demonstrated that the 'cusp of viability' for cells dependent on diffusion alone is at a depth of 1-1.5 mm from a scaffold surface, effectively limiting scaffolds to 2-3 mm in total thickness (Sailon *et al.*, 2009). Early attempts at improving flow to the core of a thick 3D scaffold by inducing convection of surrounding medium, e.g. rotational bioreactors (Freed *et al.*, 1993, 1999; Freed and Vunjak-Novakovic, 1995; Vunjak-Novakovic *et al.*, 1999), spinner flasks (Vunjak-Novakovic *et al.*, 1998, 1999), had limited success because the convection did not necessarily translate to a 'penetrating' flow that supported the core (Sikavitsas *et al.*, 2002).

More recent and more successful is the flow-perfusion bioreactor, described by Mikos and others (Bancroft *et al.*, 2003; Sailon *et al.*, 2009). The flow-perfusion bioreactor creates an *in vitro* environment that is arguably the closest physiological parallel of native bone: Cells seeded on porous scaffolds are in constant contact with the infused medium and are thereby ensured adequate oxygen delivery and satisfactory removal of waste products. Fluid flow has been shown to impart fluid shear forces on the cells, which has salutary effects on cellular growth and osteogenic differentiation (Bancroft *et al.*, 2002, 2003; Holtorf *et al.*, 2005). However, while closely simulating *in vivo* mechanobiology, the system still retains many of the benefits of an *in vitro* model, including the ability to modulate the biochemical or mechanical cues that influence cell growth and function.

A successful bone tissue-engineering system must address the need for biomimetic scaffolding that is both osteoconductive and osteoinductive as well as chemotransportative flow that will sustain thick 3D constructs and impart mechanical forces similar in magnitude to physiological events. In this study we describe our system, which was custom-designed to meet these criteria. Osteoconductive hydroxyapatite-tricalcium phosphate scaffolds were fashioned with specific porosity to permit chemotransportative flow of osteoinductive media and to create a favourable biomechanical microenvironment that further augments osteoinduction. Finite volumetric analysis and computational fluid dynamics (CFD) were employed to describe the oxygen delivery and fluid shear stresses in the system. These results were used to make design modifications in scaffold architecture that improved oxygen delivery while maintaining physiological levels of shear stress. Thus, both bioreactor and scaffolds resulted from the evolutionary outgrowth of the native structure and function of bone and the design requirements crucial to successful experimentation.

2. Materials and methods

2.1. Scaffold design and preparation

Scaffolds were prepared by an aqueous-phase, low-temperature solid freeform fabrication technique, as previously described (Figure 1) (Xie *et al.*, 2006). Milled hydroxyapatite (HA) and tricalcium phosphate (TCP) powders (Riedel-de Haën, Germany) were suspended in aqueous solution to create a concentrated 60:40 HA-TCP colloidal ink. A programmable robotic three-axis microprinter (JL2000, Sandia National Laboratories, Albuquerque, NM, USA) was used to deposit periodic lattices (in the *x-y* plane), as defined by a CAD print pattern (RoboCAD 3.0; 3D Inks, Stillwater, OK, USA). Once a layer is completed,

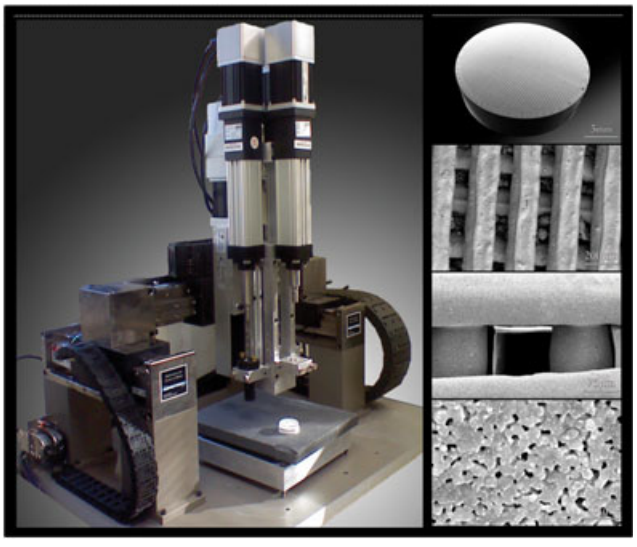

Figure 1. The bioprinter and bioprinted scaffold (photograph and SEM images)

DOI: 10.1002/term

the print head is elevated upward (along the z axis), and a perpendicular lattice is deposited. In this manner, a 3D scaffold is created by assembly of stacked lattices. Extrusion of cylindrical rods in the diameter range 50–300 μm is specified by exchangeable microtips, and pore size is determined by strut spacing. After deposition, the scaffolds are subjected to high-temperature oven firing (400°C × 1 h, 900°C × 2 h, and 1200°C × 2 h), during which the rheological agents are burned off and strut junctions are sintered. Shrinkage of 10–30% is characteristically noted during the firing process but varies predictably, based upon the ink preparation used; this shrinkage factor was anticipated in initial design parameters, such that the final dimensions of the scaffolds would grossly measure 24 mm diameter × 6 mm thickness and would be composed of 250 μm diameter struts defining 200 × 200 μm pores and a total porosity of 50%. 'Small' scaffolds for use with the bushing inserts measured 12 mm diameter × 6 mm thickness, but otherwise were identical.

While this system can be used to create scaffolds of any geometry, we investigated two architectural configurations: *onset* (struts in stacked layers directly overlying those below, leaving relatively open vertical pores with interconnecting and relatively open lateral pores (Figure 2); and *offset* (struts in stacked layers are not directly aligned, so the flow is forced to move laterally through each successive layer (Figure 3).

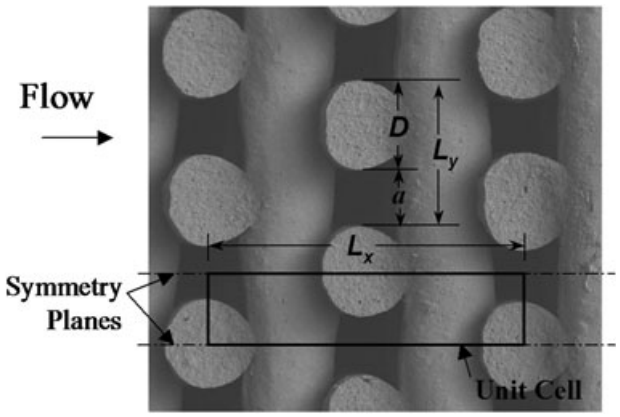

Figure 3. The offset scaffold. SEM image, with superimposed unit cell boundary, dimensions and symmetry planes: D, strut diameter; L_x, flow direction scaffold period; L_y, lateral pitch; and a, interstrut spacing

2.2. Bioreactor design

The bioreactor (Figure 4) is based upon previously described flow-perfusion devices (Bancroft *et al*., 2003; Sailon *et al*., 2009). Several materials were evaluated in prototypical devices, and ultimately Teflon®-PTFE/PYFE fluoropolymer resin (SABIC Polymershape, Jacksonville, FL, USA) was found to be ideally machinable, durable,

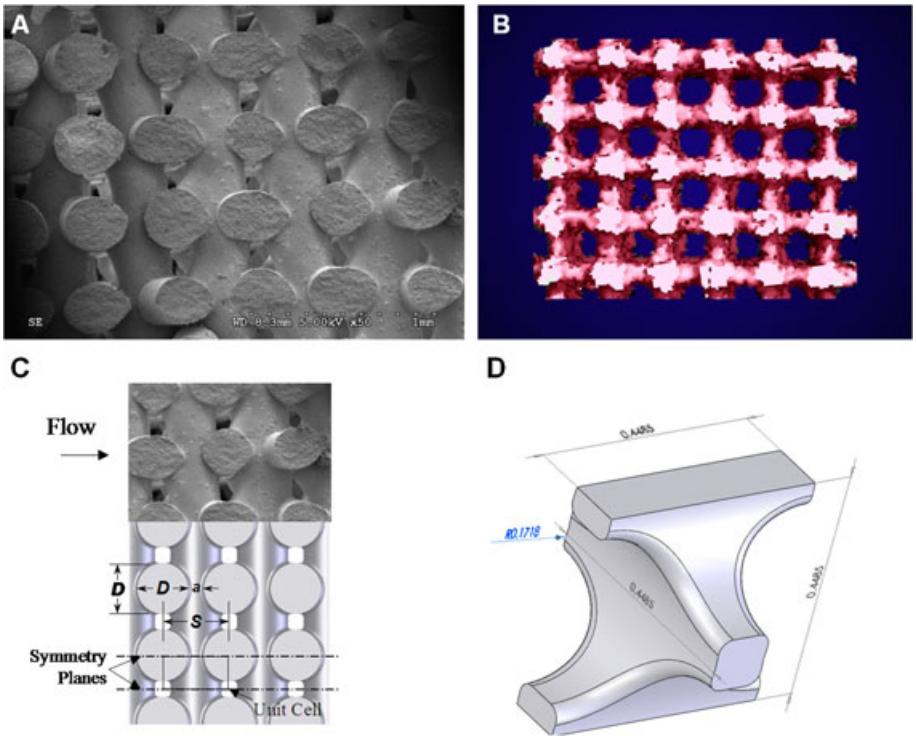

Figure 2. The onset scaffold. (A) SEM image (×50) of median section through typical onset scaffold, illustrating the perpendicular stacking of periodic lattices. (B) Micro-CT was used to generate a 3D reconstruction of the scaffold, after which subtraction of the solid HA-TCP struts allowed visualization of the interconnected pores and channels through which the medium is perfused. The orientation of the scaffold in this image is the same as in (A), i.e. struts (subtracted from view) are orientated vertically in the plane of the page and perpendicularly out of the page. The porous network is false-coloured pink for clarity. (C) Onset scaffold geometry: top, SEM image; bottom, CFD model geometry, showing strut diameter D, centre-to-centre spacing S and pore width $a = S - D$; dimensions D, S and a are assumed uniform in all dimensions (as shown for D in the figure). (D) The fluid element derived from the idealized 'onset' scaffold geometry corresponds to the shape of the porous network derived from micro-CT data

DOI: 10.1002/term

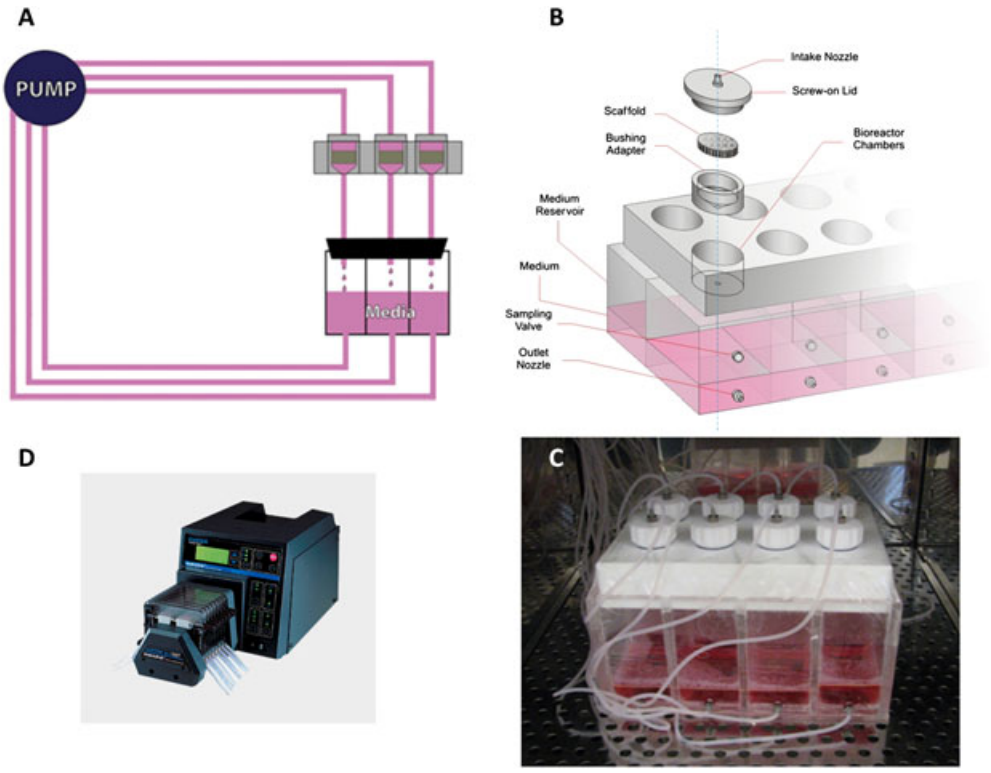

Figure 4. The flow perfusion bioreactor: (A) schematic; (B) assembly; (C) photograph; (D) peristaltic pump

biochemically inert and easy to clean. Eight equally-spaced experimental chambers were drilled to accommodate 24 mm scaffolds. The bottom of each well was tapered in order to permit flow through all regions (central or peripheral) of the porous scaffold. To accommodate scaffolds of different sizes (e.g. 12 mm diameter), we designed Teflon bushings with Viton®-75 O-rings (McMaster-Carr, Aurora, OH, USA) that would be inserted into each experimental chamber and house the scaffold while preventing flow from deviating around the scaffold. Each chamber was sealed by a threaded Teflon screw cap fitted with a Viton®-75 O-ring to ensure tight closure. A 5 mm central canal fitted with a 1/16 inch barbed male nickel-plated brass fitting (McMaster-Carr) allowed for connection of tubing.

2.3. Reservoir design

The bioreactor sits upon an acrylic reservoir (Figure 4) that houses the medium in eight separate chambers, each corresponding to the bioreactor experimental chamber directly overlying it. A gas-permeable Tegaderm^{TM} membrane (3M, St. Paul, MN, USA) is used to hermetically seal the junction between the bioreactor and reservoir. The separate reservoir chambers allow each experimental circuit to function independently (e.g. different experimental conditions or time points). Sampling ports with hermetically sealed Teflon elastic membranes allow for longitudinal sampling of medium in order to detect ion or protein concentrations. Each chamber in the reservoir is large enough to accommodate up to 100 ml of medium, which may be adequate for several weeks. For longer experiments, the medium may be removed and replaced via the sampling valves.

2.4. Multi-channel peristaltic pump and tubing

Gas-permeable platinum-cured silicone tubing (ID 0.89 mm, Cole-Parmer) was utilized for the 'extracorporeal' tubing, with a more durable neoprene (PharMed®) tubing (ID 0.89 mm; Cole-Parmer) preferred for the section that contacts the pump roller-head mechanism (Bancroft *et al.*, 2003). An eight-channel peristaltic pump with a four-head roller (Manostat-Carter, Barnant Co.) allowed perfusion in the range 0.26–14.8 ml/min (0.074 ml/revolution, 3.5–200 revolutions/min, 0.89 mm diameter tubing). Because the pump head rotates at one speed across all tubing channels, only one speed of perfusion may be evaluated per experiment.

2.5. Flow-perfusion circuit design

Each experimental chamber operates in its own, independent circuit (Figure 4). The pump draws medium from the reservoir chamber and delivers it, at the specified rate, through the screw cap to the experimental chamber. The chamber itself is completely filled with medium, such that the scaffold is in constant contact with medium on both surfaces (top and bottom). Because the scaffold is press-fitted into the chamber, the medium is constrained to flowing through the porous network of the scaffold, and non-perfusing flow is eliminated. The medium exits the

DOI: 10.1002/term

chamber through the bottom fitting in dropwise fashion to the medium reservoir below, and is recycled. The drops are visible through the clear walls of the reservoir chambers, serving as a confirmation of flow during the experiment.

2.6. System assembly

The bioreactor, bushing inserts, caps and reservoir were washed in 70% ethanol and subjected to plasma-phase H_2O_2 (Sterrad) processing for sterilization. Tubing and HA-TCP scaffolds were sterilized by autoclave. All components were assembled in a laminar-flow biosafety cabinet and transferred to a sterilized tissue-culture incubator. The tubing was passed through the equipment port on the back of the incubator and positioned within the roller-pump assembly.

2.7. Analytical methods

Computational fluid dynamics (CFD) modelling was applied to both onset and offset scaffolds to qualitatively and quantitatively measure effective pore diameter and predict mean velocity magnitude, mean wall shear stress, superficial velocity, pressure and permeability in flow perfusion. Briefly, GAMBIT meshing software (ANSYS Inc., Canonsburg, PA, USA) was utilized to organize the volume of space between scaffold struts into a tetrahedral meshwork. Algorithms applying equations used to describe the motion of fluid flow, viz. the Navier–Stokes equations, were then applied to the meshwork to generate trajectories, using FLUENT software (ANSYS). The viscous stress tensor ($\bar{\bar{\tau}}$) was evaluated using Newton's law of viscosity $\bar{\bar{\tau}} = \mu\left[\nabla\bar{v} + \nabla\bar{v}^T\right]$, where $\bar{\bar{\tau}}$ is the viscuous stress tensor, T represents the transposed. Oxygen uptake by the cells was estimated using Michaelis–Menten kinetics:

$$OCR = V_{max} \cdot \frac{C}{K_m + C}$$

where OCR denotes the oxygen consumption rate, V_{max} is the maximum oxygen uptake rate, C is the concentration of oxygen and K_m is the Michaelis–Menten constant.

2.7.1. Assumptions and limitations

The onset scaffold was analysed assuming symmetry of struts around the centre planes through each scaffold strut, and assuming that the flow field is steady and periodic (the same for each layer of scaffold) and the pressure drop relative to the start of any layer of scaffold is also periodic (the same for each layer of scaffold). Therefore, a unit cell has a width that is half of the strut spacing ($S/2$) and length equal to one layer thickness of the scaffold (S) (Figure 2). Two cases were calculated, one representing the geometry in the scanning electron microscopy (SEM) image and the second scaffold with a similar strut diameter but much wider strut spacing ('wide'). The offset scaffold was analysed on a somewhat larger representative scaffold cell, because successive layers are offset by half of the scaffold lateral pitch (Figure 3). In the offset case there are symmetry planes bisecting the struts in successive layers, so the minimum unit cell size, taking advantage of all symmetry, is half of the strut spacing laterally and two layers long, corresponding to $L_y/2 \times L_x$ in Figure 3. Scaffold dimensions were taken as averages from SEM images of a cleavage plane, yielding estimates of diameter, strut pitch and layer length. Dimensions were also taken from virtual sections through lower-resolution micro-computed tomography (micro-CT) images, yielding estimates of strut pitch and layer length. There were some significant differences between the measurements using the two imaging modes, which could be attributed to manufacturing variability. The geometrical parameters are given in Table 1.

The medium was assumed to be a Newtonian fluid. Uniform axial velocity and constant oxygen concentration at the inlet was assumed. Flow was laminar and symmetrical across a quarter unit cell and multiple unit cells, and the pressure drop was periodic across unit cells stacked in the direction of flow. Boundary cells were assumed to not significantly affect internal flow.

Medium entering the constructs was assumed to be partly equilibrated with 20% oxygen at atmospheric pressure, giving an inlet concentration of 130 μμ. Constants in the Michaelis–Menten kinetic model were not available for these cells, so they were derived from a model of oxygen mass transport to hepatocytes in a perfusion bioreactor (Roy *et al.*, 2001). Since hepatocytes have a relatively high metabolic rate, V_{max} was reduced from the published value (4×10^{-10} kM/m^2/s) to 1.25×10^{-10} kM/m^2/s. K_m was set to 55 μμ to account for reduced oxygen consumption in mesenchymal stem cells with hypoxia (Lavrentieva *et al.*, 2010).

2.8. Cell seeding and culture methods

Autoclaved HA-TCP scaffolds are hydrophilic and take up aqueous solutions easily. Two cell populations were used

Table 1. Characteristics of the model for finite volumetric analysis

Geometry	D (μm)	S (μm)	a (μm)	k (m^2)	c (m^{-1})	c_2 (m)
Onset	343.5	448.5	105	1.15×10^{-10}	256 000	2.95×10^{-5}
Offset	250	600	350	6.04×10^{-10}	128 000	7.71×10^{-5}

Geometry	D (μm)	L_x (μm)	L_y (μm)	A (μm)	k (m^2)	c (m^{-1})	c_2 (m)
Offset	298.7 ± 10.2	917.3 ± 102.4	453.8 ± 24.8	155.1	3.30×10^{-10}	144 100	4.36×10^{-5}

DOI: 10.1002/term

to validate the system: human adipose-derived mesenchymal stem cells (hASCs), as a less-differentiated population; and MC3T3-E1 pre-osteoblastic cells (Riken Cell Bank, Ibaraki, Japan) as a more-differentiated population. The cells were resuspended in Dulbecco's modified eagle's medium (DMEM; Lonza, Allendale, NJ, USA) at a concentration equivalent to the desired seeding density (for these experiments, the cellular concentration was standardized at 4×10^6 cells/cm^3). Cell suspension was administered to scaffolds in dropwise fashion in clockwise concentric circular passes to the point of scaffold saturation. Approximately 1.02 ml cell suspension was required (see Results section 3.3, below). To allow for initial cellular adhesion, the scaffolds were left undisturbed for 12 h in a cell-culture incubator (37°C humidified environment with 5% CO_2) prior to being loaded in the bioreactor chambers for dynamic culture. Extra medium in close proximity to the scaffolds prevented scaffold dessication during this interval. The cell-seeded scaffolds were then loaded into the bioreactor and subjected to continuous perfusion at a rate of 1 ml/min. For static culture controls, seeded scaffolds were maintained in six-well tissue-culture plates with enough medium to cover the scaffold in its entirety (10 ml). The medium was changed every other day to remove waste products of cell metabolism and to provide fresh growth supplements. IRB and IACUC ethical approval was not required for this project.

2.9. Cell viability and function

Scaffolds were harvested from flow-perfusion culture at day 10. Cellularity was imaged using a Zeiss EVO 50 scanning electron microscope with a backscattered electron image detector and an environmental secondary electron detector (Carl Zeiss, Thornwood, USA).

Cellular viability was assessed by fluorospectrophotometric DNA quantification, using a Picogreen DNA Quantification Kit (Molecular Probes, Seattle, WA, USA). Cellular activity was also assessed longitudinally by collecting medium from each reservoir and analysing glucose concentration by the UV Method (R-Biopharm, Marshall, MI, USA). Cellular differentiation of the hASCs towards the osteogenic lineage was examined using an alkaline phosphatase colorimetric assay (Du *et al.*, 2008). Each assay was performed in duplicate. All data are presented as mean ± standard error (SE) of the mean. A one-way analysis of variance (ANOVA) with Tukey–Kramer *post hoc* analysis was performed. Significance was considered to be $p < 0.05$.

3. Results

3.1. Computer modelling of shear stress and oxygen transport

Using inflow velocity of 1 ml/min, the mean velocity magnitude between adjacent struts in the scaffold was 0.63 mm/s in the onset scaffolds and 0.43 mm/s in the offset scaffolds. The greater velocity seen in the onset scaffolds correlated with an increased wall shear stress (0.377 dynes/cm^2 for the onset scaffolds vs 0.212 dynes/cm^2 for the offset scaffolds) (Table 2).

For the onset scaffold, the highest shear stress is located on the scaffold struts at the locations of maximum flow restriction, and shear stress is essentially zero in the lateral pores between each strut (Figure 5).

For the offset scaffold, at the same flow rate and scaffold diameter, the superficial velocity is the same, 0.0001474 m/s, but due to the different scaffold structure, the pressure gradient and shear stresses will be different, and lower due to the higher permeability, which we attribute to wider strut spacing (Figure 5).

Zones of stagnation with reduced oxygen delivery (relative hypoxia) developed between the extrusions; the slower the flow, the larger are the zones of stagnation (Figure 6).

3.2. Cell viability and function

Each scaffold was able to retain a reproducible volume of cell suspension dependent on its size, architectural configuration and composition (e.g. 1.02 ± 0.07 ml for a 60:40 HA-TCP 24 mm diameter × 6 mm thickness scaffold with 250 μm struts; and 250 × 250 μm pores in stacked 'onset' configuration). Therefore, the total number of cells seeded can be controlled by varying the cell concentration of the suspension. For the purposes of these experiments, a universal seeding density of 4×10^6 cells/cm^3 was employed.

In separate experiments, various flow rates were evaluated to determine which rates were 'too fast' to allow for cellular adhesion; the rate of 1 ml/min featured negligible loss of cells (data not shown) and was chosen for these experiments. Cellular adhesion was not improved with longer periods of static culture (i.e. > 12 h) prior to institution of flow (data not shown).

Also in separate experiments (data not shown), continuous dynamic cell culture was continued through a period of 8 weeks, with medium exchanged under sterile conditions through the sampling ports in the reservoir on a weekly or bi-weekly basis. At 8 weeks, however, we

Table 2. Properties of fluid flow through onset and offset scaffolds, as predicted by computational fluid dynamics

	Onset	Offset
Effective pore diameter (μm)	105	155
Inlet flow rate (ml/min)	1	1
Mean velocity magnitude (mm/s)*	0.63	0.43
Mean wall shear stress (dynes/cm^2)	0.377	0.212
Superficial velocity (mm/s)	0.1474	0.1474
Pressure (Pa)	7.67	2.87
Pressure gradient (Pa/m)	1280	478
Permeability (m^2)	1.15×10^{-10}	3.03×10^{-10}

*Mean velocity magnitude represents the velocity between adjacent struts.

DOI: 10.1002/term

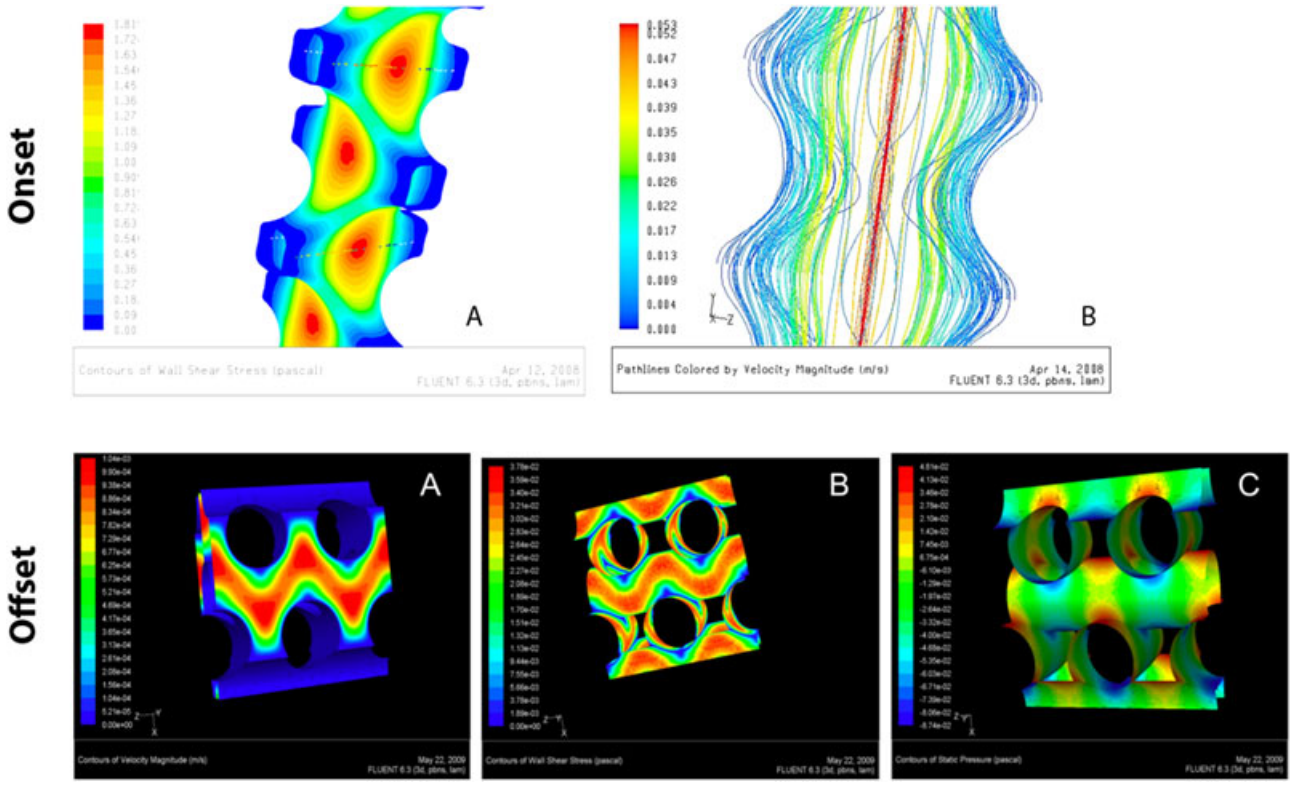

Figure 5. Finite volumetric analysis of shear stress in onset and offset scaffolds. Top row, onset scaffold (A) wall shear stress plot (taken at –25450 Pa/m); (B) velocity plot (taken at –33923 Pa/m). Bottom row, offset scaffold (A) velocity (0–1.04 × 10^{-3} m/s); (B) wall shear stress (0–0.378 dynes/cm^2); (C) pressure

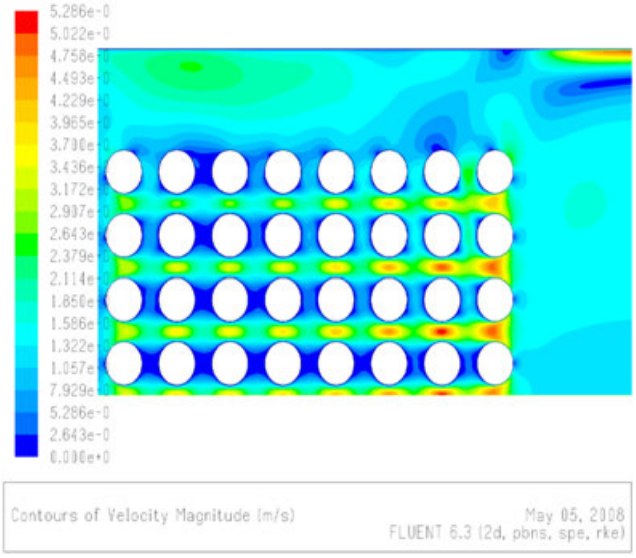

Figure 6. Finite volumetric analysis of oxygen delivery in the onset scaffold. Notice blue 'shadowing' beneath each strut, indicating areas of relative hypoxia

observed mechanical breakdown of the tubing section within the rotary pump head, which resulted in system contamination. Prior to this event, the system's hermetic seal was preserved, and there were no obvious signs of infection. It may be possible to extend the duration of long-term culture by pre-emptively exchanging the tubing sterilely, but we have not yet attempted this intervention.

After a 10 day culture period, SEM revealed increased cellular proliferation and cellular interaction in flow-perfused samples compared with static controls. Moreover, cell density was maintained throughout the scaffold in flow perfusion but localized to the periphery in static culture. Furthermore, there was added value in using the offset scaffold (Figure 7). When cellularity was quantified by DNA pico-green assay, the increase in cell proliferation in flow perfusion, greater with the offset scaffold, was confirmed: 1183.63 ± 34.79 ng/l in static (offset); 1871.71 ± 24.38 ng/l for onset scaffolds in flow; and 2794.50 ± 52.90 ng/l for offset scaffolds in flow (static offset vs flow onset, $p < 0.01$; flow onset vs flow offset, $p < 0.01$; static offset vs flow offset, $p < 0.01$) (Figure 8).

To observe osteogenic differentiation of the hASCs under flow perfusion, an alkaline phosphatase colorimetric assay was employed. Enzymatic activity, measured as mM *p*-nitrophenol produced/g scaffold, increased for both onset and offset scaffolds in flow by day 10 compared with static controls: 1.17 ± 0.94 mM/g (static offset); 6.26 ± 3.00 mM/g (flow onset); and 5.23 ± 1.76 mM/g (flow offset): static offset vs flow onset, $p < 0.01$; flow onset vs flow offset, not significant; static offset vs flow offset, $p < 0.01$ (Figure 8).

4. Discussion

Our laboratory has developed a flow-perfusion bioreactor system, complete with novel porous HA-TCP scaffolds

DOI: 10.1002/term

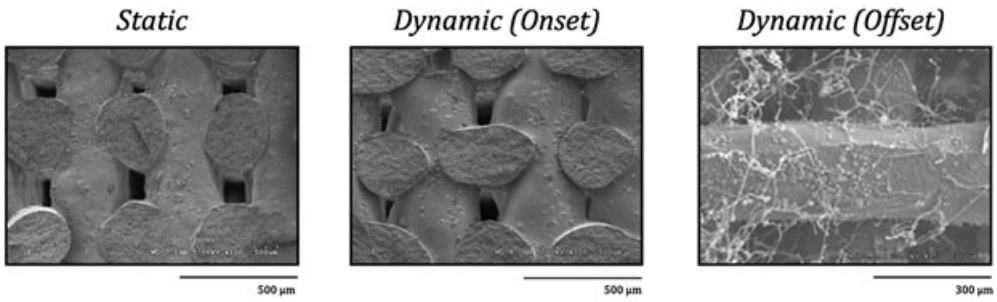

Figure 7. SEM images following 10 days of dynamic culture of MC3T3-E1 demonstrate higher cell density, dendritic phenotype and extracellular matrix production in the 'offset' scaffolds

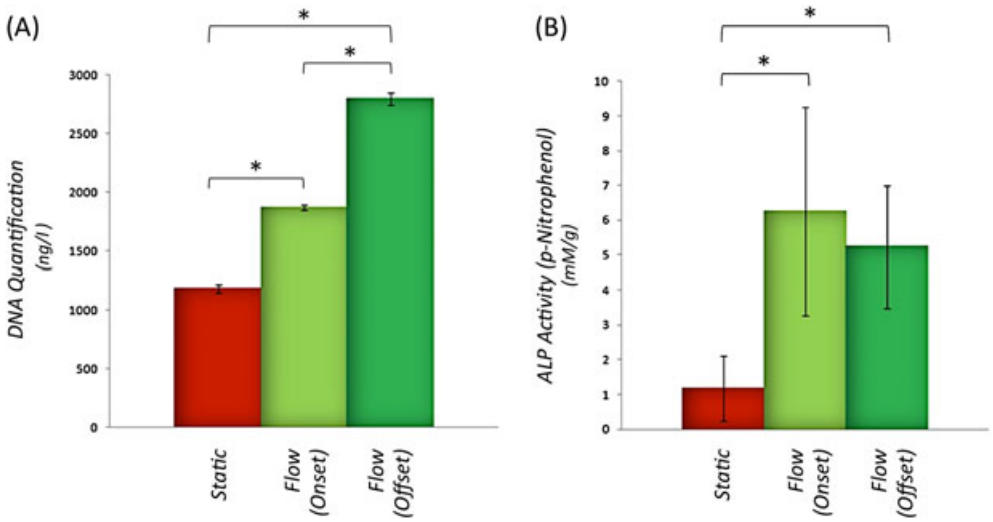

Figure 8. (A) DNA quantification and (B) alkaline phosphatase activity normalized to DNA quantity, following a 10 day dynamic culture period of hASCs. *Statistically significantly difference ($p < 0.01$)

intended to mimic the native environment of bone. Together, these allow cell culture in relatively thick 3D scaffolds, typified by survival and proliferation of cells throughout the scaffold in the long term (1–2 months). All samples remained free from infection.

Computational fluid dynamics predicted higher mean flow velocity in the onset scaffold and therefore, in keeping with consensus in the literature, we would expect greater cellular proliferation but lesser osteogenic differentiation in the offset scaffolds, compared to onset, because of a lower mean shear stress value (Zhao *et al.*, 2007). Our experimental results *in vitro* corroborated these predictions: Specifically: (a) in static culture there was relatively higher cellular density on the periphery of the scaffold and a paucity of cells in its core; (b) in fluid flow (dynamic culture) the cellular density in the core improved relative to static culture; and (c) greater cell viability and proliferation was observed in offset scaffolds compared to onset scaffolds, as measured by DNA quantification. Cellular distribution and proliferation were measured by counting and DNA quantification. Viability was not directly quantified, which may be considered a limitation of the present investigation.

Notably, computational models described relative zones of stagnation in the onset scaffold beneath each strut. The degree of hypoxia worsened with slower rates of fluid flow (Figure 6). Computational fluid dynamics (CFD) of onset vs offset scaffold designs suggest that fluid flow and shear stress improves within these zones with an offset strut arrangement. We hypothesize that oxygen delivery in these zones would similarly be improved, although further FEA modelling of oxygen delivery for the offset scaffold has not yet been performed. However, *in vitro* results corroborate improved cellular distribution and proliferation in these regions.

To our knowledge, these specific onset and offset designs are novel and unique to this project. However, these scaffolds are based upon the common design principles of optimizing fluid flow and chemotransportation to cells. As onset and offset do not distinctly parallel structures in nature, it may be incorrect to dub either as being 'biomimetic'; however, to the extent that offset scaffolds optimize fluid flow and chemotransportation, they may be considered more suitable for bone-engineering applications.

Our SEM imaging demonstrated that cells adhered to scaffold struts, proliferated and assumed a dendritic phenotype. These podocytic extensions appear to contact other cells, and we suspect that many of these contact points are gap junctions that permit intercellular

DOI: 10.1002/term

communication, as is observed between native bone cells *in situ*. This is an area of ongoing investigation.

5. Conclusion

The flow-perfusion system is an *in vitro* physiological parallel to an *in vivo* process: The flow of medium through the porous scaffold is in many ways similar to the natural fluid shift within native bone's lacunocanalicular network, that occurs in response to a deformational force: specifically, the convection imparts a fluid shear stress that is perceived by the embedded cell, just as *in vivo*, and the fluid flow improves chemotransportation. However, while closely simulating *in vivo* mechanobiology, the system retains all the benefits of an *in vitro* model, including the ability to precisely control environmental clues to guide and enhance cell function. Levels of mechanical strain can be chosen and set, and utilizing small 'microstrains' at high frequency of oscillation over a prolonged course can greatly enhance cellular response. Indeed, both bioreactor and osteoconductive/osteoinductive scaffolds resulted from the evolutionary outgrowth of the native structure/function of bone and the design requirements crucial to successful experimentation. Specifically, finite element analysis results were used to make scaffold design modifications that could achieve a desired range of shear stress on the scaffold surface while maintaining a good superficial velocity for maintenance of mass transport. Thus, the flow-perfusion bioreactor provides an ideal environment to study bone biology and to develop bone-engineering protocols.

Acknowledgements

This work was graciously supported in part by the Lyndon Peer Research Fellowship, administered by the Plastic Surgery Educational Foundation (PSEF); the Bernd Spiessl Research Award, administered by the American Society of Maxillofacial Surgery (ASMS) through the courtesy of Synthes CMF; the PSEF Basic Science Research Grants; the Alpha Omega Alpha Carolyn L. Kuckein Research Fellowship; the 2008 Association of Academic Plastic Surgeons (AAPS) Academic Scholar Award; and the 2010 AOCMF Award. Much appreciation is due to Umberto Allori and James Vertolli for assistance with the bioreactor design and manufacturing, respectively.

Conflict of interest

The authors have declared that there is no conflict of interest.

References

Allori AC, Sailon AM, Pan JH, *et al*. 2008a; Biological basis of bone formation, remodeling, and repair – part III: biomechanical forces. *Tissue Eng B Rev* **14**(3): 285–293.

Allori AC, Sailon AM, Warren SM. 2008b; Biological basis of bone formation, remodeling, and repair – part II: extracellular matrix. *Tissue Eng B Rev* **14**(3): 275–283.

Bancroft GN, Sikavitsas VI, Mikos AG. 2003; Design of a flow perfusion bioreactor system for bone tissue-engineering applications. *Tissue Eng* **9**(3): 549–554.

Bancroft GN, Sikavitsas VI, van den Dolder J, *et al*. 2002; Fluid flow increases mineralized matrix deposition in 3D perfusion culture of marrow stromal osteoblasts in a dose-dependent manner. *Proc Natl Acad Sci USA* **99**(20): 12600–12605.

Cowin SC, Moss-Salentijn L, Moss ML. 1991; Candidates for the mechanosensory system in bone. *J Biomech Eng* **113**(2): 191–197.

Du D, Furukawa K, Ushida T. 2008; Oscillatory perfusion seeding and culturing of osteoblast-like cells on porous β-tricalcium phosphate scaffolds. *J Biomed Mater Res A* **86**(3): 796–803.

Freed LE, Pellis N, Searby N, *et al*. 1999; Microgravity cultivation of cells and tissues. *Gravit Space Biol Bull* **12**(2): 57–66.

Freed LE, Vunjak-Novakovic G. 1995; Cultivation of cell–polymer tissue constructs in simulated microgravity. *Biotechnol Bioeng* **46**(4): 306–313.

Freed LE, Vunjak-Novakovic G, Langer R. 1993; Cultivation of cell–polymer cartilage implants in bioreactors. *J Cell Biochem* **51**(3): 257–264.

Fritton SP, McLeod KJ, Rubin CT. 2000; Quantifying the strain history of bone: spatial uniformity and self-similarity of low-magnitude strains. *J Biomech* **33**(3): 317–325.

Gosain AK, Song L, Riordan P, *et al*. 2002; A 1-year study of osteoinduction in hydroxyapatite-derived biomaterials in an adult sheep model: part I. *Plast Reconstr Surg* **109**(2): 619–630.

Holtorf HL, Jansen JA, Mikos AG. 2005; Flow perfusion culture induces the osteoblastic differentiation of marrow stroma cell–scaffold constructs in the absence of dexamethasone. *J Biomed Mater Res A* **72**(3): 326–334.

Lavrentieva A, Majore I, Kasper C, *et al*. 2010; Effects of hypoxic culture conditions on umbilical cord-derived human mesenchymal stem cells. *Cell Commun Signal* **8**: 18–26.

Nguyen PD, Lin CD, Allori AC, *et al*. 2009; Establishment of a critical-sized alveolar defect in the rat: a model for human gingivoperiosteoplasty. *Plast Reconstr Surg* **123**(3): 817–825.

Roy P, Baskaran H, Tilles AW, *et al*. 2001; Analysis of oxygen transport to hepatocytes in a flat-plate microchannel bioreactor. *Ann Biomed Eng* **29**(11): 947–955.

Sailon AM, Allori AC, Davidson EH, *et al*. 2009; A novel flow-perfusion bioreactor supports 3D dynamic cell culture. *J Biomed Biotechnol* 873816.

Scherberich A, Galli R, Jaquiery C, *et al*. 2007; Three-dimensional perfusion culture of human adipose tissue-derived endothelial and osteoblastic progenitors generates osteogenic constructs with intrinsic vascularization capacity. *Stem Cells* **25**(7): 1823–18239.

Sikavitsas VI, Bancroft GN, Mikos AG. 2002; Formation of three-dimensional cell/polymer constructs for bone tissue engineering in a spinner flask and a rotating wall vessel bioreactor. *J Biomed Mater Res* **62**(1): 136–148.

Simon JL, Michna S, Lewis JA, *et al*. 2007; *In vivo* bone response to 3D periodic hydroxyapatite scaffolds assembled by direct ink writing. *J Biomed Mater Res A* **83**(3): 747–758.

Simon JL, Rekow ED, Thompson VP, *et al*. 2008; MicroCT analysis of hydroxyapatite bone repair scaffolds created via three-dimensional printing for evaluating the effects of scaffold architecture on bone ingrowth. *J Biomed Mater Res A* **85**(2): 371–377.

Vunjak-Novakovic G, Martin I, Obradovic B, *et al*. 1999; Bioreactor cultivation conditions modulate the composition and mechanical properties of tissue-engineered cartilage. *J Orthop Res* **17**(1): 130–138.

Vunjak-Novakovic G, Obradovic B, Martin I, *et al*. 1998; Dynamic cell seeding of polymer scaffolds for cartilage tissue engineering. *Biotechnol Prog* **14**(2): 193–202.

Weinbaum S, Cowin SC, Zeng Y. 1994; A model for the excitation of osteocytes

DOI: 10.1002/term

by mechanical loading-induced bone fluid shear stresses. *J Biomech* **27**(3): 339–360.
Weinbaum S, Guo P, You L. 2001; A new view of mechanotransduction and strain amplification in cells with microvilli and cell processes. *Biorheology* **38**(2–3): 119–142.
Xie B, Parkhill RL, Warren WL, *et al*. 2006; Direct writing of three-dimensional polymer scaffolds using colloidal gels. *Adv Funct Mater* **16**(13): 1685–1693.
Zhao F, Chella R, Ma T. 2007; Effects of shear stress on 3D human mesenchymal stem cell construct development in a perfusion bioreactor system: experiments and hydrodynamic modeling. *Biotechnol Bioeng* **96**(3): 584–595.

DOI: 10.1002/term